Acta Crystallographica Section D
Biological Crystallography
ISSN 0907-4449

Comparison of lysozyme structures derived from thin-film-based and classical crystals

Eugenia Pechkova,[a,b] Victor Sivozhelezov,[a] Giuseppe Tropiano,[b] Stefano Fiordoro[a] and Claudio Nicolini[a,b]*

[a]Fondazione Elba, Via delle Testuggini, 00100 Roma, Italy, and [b]Nanoworld Institute and Biophysics Division, University of Genoa, Corso Europa 30, 16132 Genoa, Italy

Correspondence e-mail: manuscript@ibf.unige.it

Received 14 August 2004
Accepted 2 March 2005

The present report is dedicated to a systematic comparison of crystal structures produced by the nanobiofilm template method and by the classical hanging-drop vapour-diffusion method. Crystals grown by the innovative nanostructured template method appear indeed radiation-resistant even in the presence of a third-generation highly focused beam at the European Synchrotron Radiation Facility. The implications of this finding for protein crystallography are discussed here in terms of water redistribution and of the detailed atomic resolution comparative studies of the two crystal structures with or without nanobiofilm template, as emerging also from circular-dichroism and thermal denaturation studies.

1. Introduction

Lysozyme is a hydrolase enzyme (EC 3.2.1.17) which, thanks to its exceptional ease of crystallization, is frequently used as an example in protein crystallization studies, such as effects of impurities, pH, and temperature on crystallization mechanisms (Yoshizaki *et al.*, 2004; Judge *et al.*, 1998, 1999), reservoir volume to crystallization volume ratio (Forsythe *et al.*, 2002), improvement of crystal quality by magnetic field (Ataka & Wakayama, 2002), nucleation rates (Garcia-Ruiz, 2003, for review), microscopic (atomic level) mathematical modelling including statistical mechanics and lattice simulations of nucleation (Kierzek & Zielenkiewicz, 2001, for review), macroscopic mathematical modeling of crystallization kinetics (Manno *et al.*, 2003; Agena *et al.*, 1999; Bessho *et al.*, 1994), and X-ray topography analysis of crystal perfection, growth, quality, response to humidity and dislocations (Tachibana *et al.*, 2003; Hu *et al.*, 2001; Dobrianov *et al.*, 1998, 2001; Boggon *et al.*, 2000). On the other hand, lysozyme is routinely used as a test object when a new technique needs to be verified. Indeed, the double-pulse technique (thermal or concentration) was used to investigate lysozyme nucleation and adhesion (Penkova *et al.*, 2002; Tsekova *et al.*, 1999), while microfluidic techniques were evaluated with respect to crystal growth, quality and nucleation (Adachi *et al.*, 2004; Kadowaki *et al.*, 2004; van der Woerd *et al.*, 2003; Sanjoh *et al.*, 2001; Chayen *et al.*, 2001). Among the nanoscale molecular-manipulation techniques, Langmuir–Blodgett (LB) film technology has a long and successful record (for reviews, see Nicolini, 1998; Izumi *et al.*, 1998; Pepe & Nicolini, 1996; Arslanov, 1992; some recent advances are described in Bertoncello *et al.*, 2003, 2004; Bavastrello *et al.*, 2004). This has prompted us to investigate the influence of LB film on crystallization, crystal quality and eventual structure of the protein and its aqueous environment in the crystal. We initially found that LB coating on the cover slide of the common crystallization plates lead to stimulation of protein crystal growth, allowing the acceleration of the lysozyme crystal-growth rate compared with the classical vapour-diffusion method (Pechkova & Nicolini, 2001). Radiation-stable microcrystals with pronounced diffraction patterns were then reproducibly obtained by the nanotechnology-based method (Pechkova & Nicolini, 2003, and references therein) for the proteins cytochrome P450scc and human kinase CK2, for which crystallization attempts using conventional methods were unsuccessful. It is important to note that the use of microcrystals for X-ray diffraction studies requires much higher source luminosity than available by the standard sources, so a

synchrotron source was used. For the kinase, we have derived the atomic resolution structure at the ESRF microfocus beamline from miniscule protein microcrystals with diameters of 20 μm (Pechkova & Nicolini, 2004*a*; Pechkova *et al.*, 2003). This opened the road to development of a new interdisciplinary field of research that we termed nanocrystallography (Pechkova & Nicolini, 2004*b*). Apart from LB and synchrotron technologies, nanocrystallography makes extensive use of atomic force microscopy, considering that (i) the AFM images coincide with those obtained by X-ray diffraction and (ii) it is by AFM that mechanisms and kinetics of crystal growth have been successfully determined.

However, the exact mechanism by which presence of LB film accelerates and guides crystallization is not clear even though it is quite evident that the primary physical factor is the anisotropy rendered by the film to the growing crystal. This anisotropy possibly has electrostatic nature, since dipole moments of protein monomers are oriented identically in the film, which is confirmed by surface potential measurements (Pechkova & Nicolini, 2003, and references therein). This study attempts to determine whether introduction of LB film modifies the three-dimensional structure of the protein and/or the configuration of water molecules surrounding the protein. To do this, we determined the three-dimensional structure of lysozyme in the LB film-based and the classical crystals using the molecular-replacement method. Apart from the above considerations, we chose lysozyme because any improvement of the crystal quality upon LB film introduction, considering that the quality of the classical lysozyme crystals is already quite high, could imply an enormous potential of the method for not so readily crystallizable proteins. Extra small crystals of only a few micrometres in size, formerly unusable for the structural analysis, now can be used for the diffraction data collection by means of third-generation synchrotrons thanks to the introduction of microfocus beamlines. However, one cannot indefinitely compensate for small crystal size with increased beam intensity since at some stage so much X-ray energy is being deposited in a small volume that the protein structure and crystalline order will be destroyed by primary radiation damage very quickly. Primary radiation damage is linearly dependent on the X-ray dose even when the crystal is at cryogenic temperatures. Among the existing strategies against radiation damage, there are improving cooling techniques, free radical scavengers use, but also beam defocusing in order to decrease the available flux density. However, the radiation damage to crystalline proteins using X-rays remains a problem which limits the structural information that can be extracted from the sample, and only significant increase of radiation stability of the crystals can open new avenues in structural proteomics. Radiation stability was apparently induced in the crystal formed by the recently introduced nanofilm template method (Pechkova *et al.*, 2004).

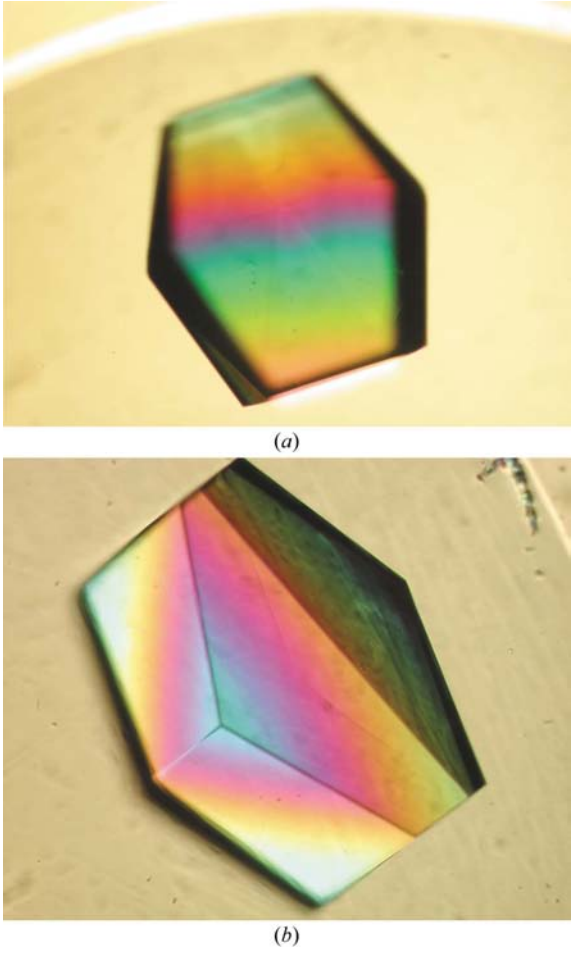

Figure 1
(*a*) Lysozyme crystal grown by classical hanging-drop method. The dimension of this typical crystal along the longest axis is 600 μm. (*b*) Lysozyme crystal grown by the nanotemplate crystallization method. The dimension of this typical crystal along the longest axis is 800 μm.

2. Methods

Chicken egg-white lysozyme protein was purchased from Sigma.

2.1. Hanging-drop crystallization method

The crystallization conditions used for the classical hanging-drop method were a 4 μl drop containing 20 mg ml^{-1} lysozyme in 25 m*M* sodium acetate buffer pH 4.5 and 0.45 *M* sodium chloride placed on the siliconized glass slide and stabilized over the reservoir containing 0.9 *M* sodium chloride in sodium acetate buffer. A photograph of a classical lysozyme crystal is shown in Fig. 1(*a*).

2.2. Nanotemplate crystallization method

The nanotemplate-based crystallization method was utilized as described in Pechkova & Nicolini (2001). Lysozyme thin film was prepared on the water-area interface and compressed to a surface pressure of 25 mN m^{-1} by means of a Langmuir–Blodgett trough (Nicolini, 1997). A protein monolayer was deposited on the siliconized glass cover slide of 20 mm diameter (Hampton Research) by the Langmuir–Schaeffer method. This highly ordered protein nanotemplate was utilized in a hanging-drop protein crystallization method modification. The drop of protein solution and the precipitant (salt) was placed on the glass slide covered by thin film nanotamplate. As in the classical hanging-drop method, the glass slide with the protein template and the drop was sealed on the crystallization plate (Limbro plate, Hampton Research) using vacuum grease. The crystallization conditions usually used for the classical hanging-drop method were applied: a 4 μl drop containing 20 mg ml^{-1} lysozyme in 25 m*M* sodium acetate buffer pH 4.5 and 0.45 *M* sodium chloride was placed on the siliconized glass slide covered with the lysozyme monolayer and stabilized over the reservoir containing 0.9 *M* sodium chloride in sodium acetate buffer. A photograph of an LB film-based lysozyme crystal is shown in Fig. 1(*b*).

2.3. Data collection and processing

Diffraction data were collected at a temperature of 100 K. Crystals were fished out from the mother liquor and frozen in a nitrogen

Table 1
Parameter comparison of reflection data, electron-density maps and three-dimensional structures between the classical and the LB crystals of lysozyme.

	Classical	LB-based
Beamline	Microfocus ID13, ESRF	
Temperature (K)	100	
Detector	MAR CCD	
Wavelength (Å)	0.9755	
Space group	$P4_32_12$	
Unit-cell parameters (Å, °)	a = 78.89, b = 78.89, c = 37.16, $\alpha = \beta = \gamma = 90$.	a = 79.21, b = 79.21, c = 37.42, $\alpha = \beta = \gamma = 90$.
Resolution range	27–1.7	
Independent reflections	13046	13598
Common (same *hkl*) reflections for classical and LB data sets	12866	
Map fragmentation† (%)	12.3 (11.2)	5.0 (5.3)
Total map/model correlation coefficient†‡	0.758 (0.755)	0.726 (0.733)
Total map/model correlation coefficient†§	0.859 (0.857)	0.891 (0.890)
R factor	0.210	0.208
R_{free} for 5% data in the set	0.283	0.274
Expected maximal error in coordinates (Å)	0.105	0.108
R.m.s.d., bonds (Å)	0.084	0.087
R.m.s.d., angles (°)	1.192	1.178
Average B factor (Å^2)	18.973	19.976
α-Helix content, residues	42	45
Quantity of water molecules resolved per lysozyme molecule at 100σ threshold	63	53
Quantity of water molecules modelled in a 60 Å diameter sphere (including those resolved)	4933	4669

† Values in parentheses are for the restricted data sets containing the 12866 reflections with same *hkl* for each data set. ‡ Water molecules not included in the model. § Water molecules included.

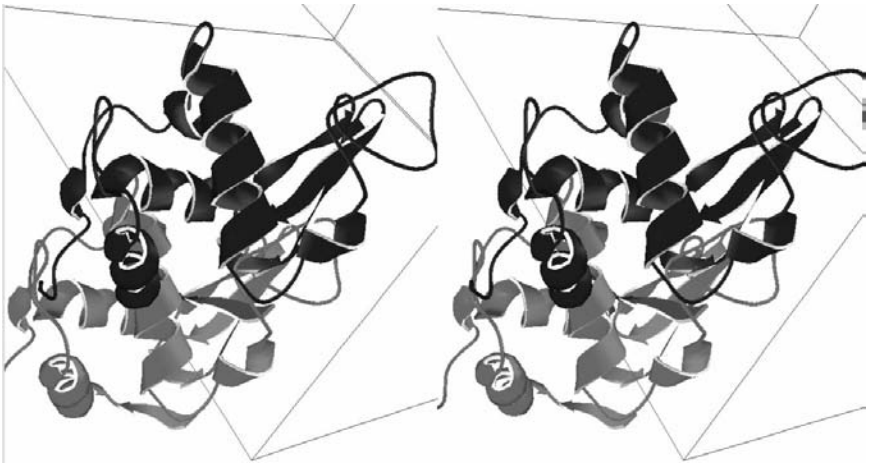

Figure 2
Stereoview of orientation of the lysozyme molecule with respect to the crystal cell. The classical structure is darker, the film-based structure is lighter. Axes are, from leftmost clockwise: y, z, x.

stream using Paraton-N (Hampton Research) as cryoprotectant. Classical and LB-film based lysozyme crystals of approximately the same dimensions and shape were used to collect two complete data sets at the Microfocus beamlineID-13 at the ESRF (beam size 20 × 20 µm). The wavelength used was 0.9755 Å and the crystal-to-detector distance was 100 mm. Crystals diffracted to a maximum resolution of 1.7 Å.

Lysozyme crystals belong to space group $P4_32_12$, with unit-cell parameters being (classical/LB-based) $a = b$ = 78.89/79.21, c = 37.16/37.42 Å. One molecule is present in the asymmetric unit. Assuming a molecular weight of approximately 14 000 Da, the V_M coefficient is about 2.09 Å.

Standard procedures of data reduction were followed using programs from the *CCP*4 suite (Wild *et al.*, 1995), *MOSFLM* and *SCALA*. The phase problem was solved using the molecular-replacement method using the software package *CNS* (Brünger *et al.*, 1998) and the three-dimensional structure was determined from the electron-density map using the software packages *QUANTA* (http://www.accelrys.com/quanta/quanta.html) *via* map skeletonization and secondary-structure determination and the package *XtalView* (McRee, 1992 *via* direct fitting of C^α atoms. Refinement was performed manually using both packages, followed by automatic restrained refinement with isotropic B factors using the *CCP*4 suite program *REFMAC*5.

2.4. Circular-dichroism measurements

Circular dichroism data of lysozymes in solution, thin protein film and dissolved crystals were taken with a Jasco J-710 spectropolarimeter at physiological ionic strength and neutral buffer (Nicolini & Baserga, 1975; Pulsinelli *et al.*, 2003).

Circular-dichroism spectra were recorded on a Jasco J-710 spectropolarimeter (Jasco, Japan) equipped with a Peltier thermostatic cell holder. All spectra were recorded in 0.05 cm path-length quartz cell under nitrogen atmosphere, using the following parameters: time constant 4 s, scanning speed 20 nm min^{-1}, bandwidth 2 nm, sensitivity 10 mdeg, step resolution 0.5 nm. The photomultiplier voltage did not exceed 600 V in the spectral region measured. The instrument was calibrated with a standard solution of (+)-10-camphosulfonic acid. Each spectrum was averaged five times in the wavelength range 250–180 nm. Samples were prepared in 15 mM phosphate buffer pH 8.0 at a protein concentration of about 0.1 mM. All the acquired spectra were corrected for the baseline and normalized to the amino-acid concentration in order to calculate the mean residual molar ellipticity (deg cm^2 dmol^{-1}).

3. Results and discussion

We choose two typical crystals, obtained by the classical hanging-drop (Fig. 1*a*) and nanotemplate crystallization methods (Fig. 1*b*). The crystal grown in the presence of the LB film is larger (800 µm), than that by classical method (600 µm) due to the accelerated growth as previously reported (Pechkova & Nicolini, 2001). The two crystals have approximately the same shape.

To facilitate comparing the differences in the structures derived from classical and LB-based crystals, we assessed the overall characteristics of crystals by comparing the initial reflection data, the maps derived from them and the three-dimensional structures obtained. These results are summarized in Table 1.

Generally, the difference between the structures of lysozyme molecule itself is very small, only about 0.28 Å r.m.s. difference between the LB-based and the classical structures when they are superimposed after fitting the C^α traces into the electron-density maps. After manual refinement, this difference reduces to 0.17 Å, but then increases to 0.24 Å after automatic restrained refinement. However, the lysozyme molecules are oriented differently with

respect to the crystal axes (Fig. 2), which might be related to differences in hydrogen bonding with water molecules. The unit-cell parameter *c* (37.16 Å in the classical *versus* 37.42 Å in the LB crystals, which is 0.7% difference) indicates that either packing of the molecules or their conformation (which is less likely considering the quoted r.m.s.d. values) may differ between the classical and the LB crystals. Anyway, both of these factors should affect hydrogen-bonding patterns at the protein/water interface and thus patterns of water molecules around the protein.

This prompted us to analyze the arrangement of water molecules around the lysozyme molecule, which indeed exhibited a much larger difference. Indeed, a smaller number of water molecules were resolved for the LB crystal at high threshold compared with the classical crystal. The observed *R* factors are sufficiently low to allow such a comparison. Besides, comparison of *R* factors (both working and free), *B* factors, positional errors in coordinates and r.m.s. values for bond lengths and bond angles shows that values of these parameters are very similar between the classical and the LB data sets, which rules out insufficient precision of structure determination or different qualities of film-based and LB-based crystals as sources of error in comparing the patterns of lysozyme's aqueous surroundings between the LB and the classical crystals.

It follows from our data that even though three-dimensional structures of lysozyme in the LB and classical crystals are the same, water molecule arrangements around the protein widely differ. The validity of this observation is supported by the fact that the lysozyme structure remains essentially the same even if the solvent content is extremely low, as in the case of low-humidity crystals (Madhusudan *et al.*, 1993).

To check if the observed differences in arrangement of water molecules could be caused by different numbers of reflections in the classical and LB data sets leading to different heights of electron-density peaks and eventually to artifacts in water-molecule assignments, we selected reflections having the same *hkl* indices for both classical and LB data sets and recalculated the values of map fragmentation and map/structure correlation coefficients. We expressed map fragmentation as a fraction of electronic density contained in fragments other than the largest fragment of the map, determined by the map skeletonization procedure of the software package *QUANTA*. Both parameters remained practically unchanged for the restricted data sets compared with the original data sets, which we believe to rule out the discussed artifact.

Table 2
Secondary structure of water-dissolved lysozyme crystals derived from modified vapour-diffusion method with (LB crystal) and without (classical crystals) lysozyme thin film used as nanotemplate.

In the table, the percentages of various types of secondary structure are indicated. For reference, the percentage of α-helix in lysozyme thin film is 40% (Pechkova *et al.*, in preparation).

	α-Helix	β-Sheet	β-Turn	Random coil
LB crystals	36.6	25.2	7.4	30.8
Classical crystals	28.4	28.6	10.5	32.5

The high (100σ) threshold for detecting water molecules was chosen to be certain that all of the resolved water molecules immediately adhere to the protein surface. To estimate how water will surround the lysozyme molecule in a crystal, water molecules were modeled by expanding the already resolved water layer, to fill a 60 Å diameter sphere for both the classical and the LB crystals. Such a modelling technique repeats the surface topology of protein and the adherent water layer and is therefore suitable for modeling water in a crystal. At this point, the difference in water content is estimated to be about 6% smaller for LB (4669 against 4933 molecules), which is augmented by the fact that the unit-cell volume is somewhat larger (235 against 231 nm^3) for the LB crystals. Indeed, it follows from these values that the water density in the LB crystals should be about 7.5% smaller than for the classical crystals, suggesting a higher degree of ordering, as follows from the known fact that ice is less dense than water. How this ordering is conferred to the water in lysozyme crystals is not clear. One may suggest that the residues belonging to the film affect ordering of the lysozyme molecules, either within the film or upon partial dissociation of a fragment from the film. That, however, is unlikely since the space group of the crystal does not change upon introduction of the film. Alternatively, the film could create a lattice-like pattern of electrostatic potential that could affect the assembly of proteins in the immediate vicinity of the film and/or act *via* improved hydrogen bonding between the water molecules. In the latter case, a tendency to higher hydrogen bonding within the lysozyme molecule should be observed, since water molecules, being involved in more hydrogen bonding in bulk water, will be less prone to disturb intraprotein hydrogen bonding. For proteins, a higher level of intraprotein hydrogen bonding typically leads to increased secondary-structure content (Felts *et al.*, 2004, and references therein), particularly with respect to α-helices (Aurora *et al.*, 1997; Grandi *et al.*, 1981) that are largely held together by hydrogen bonds. Indeed, slightly increased α-helicity is observed for the LB crystal (Fig. 3).

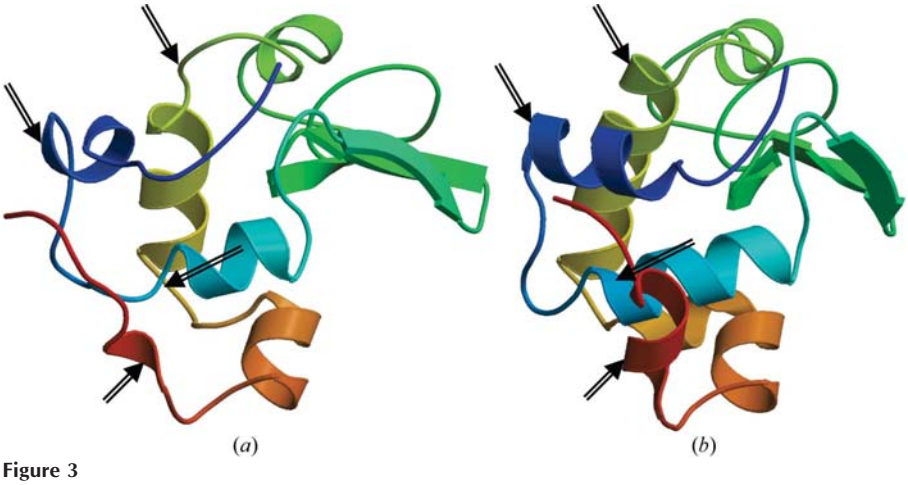

Figure 3
Secondary structures obtained for the classical (*a*) and the film-based (*b*) structures. The apparent differences are indicated by arrows.

As already specified, different hydrogen-bonding patterns of protein with water is in good agreement with the observed drastic difference in orientation of protein with respect to the crystal axes. However, we cannot at this point determine which of these phenomena is the cause and which is the effect. Indeed, different mechanisms may be proposed explaining our data. One is the change of protein reorientation within the crystal cell caused by electrostatic anisotropy and mediated by hydrogen bonding while in another it is hydrogen bonding is mediated by protein reorientation, which occurs in the immediate vicinity of the LB film surface. As seen from Fig. 2, the effect of

LB film leads mostly to the shift along the z axis, of a distance of about 20 Å, and also by about 5° rotation around the z axis. This shows that the orientation rendered by the film is considerable enough to counteract crystal forces.

The spectropolarimetric data derived from Langmuir–Blodgett-based and classical crystals dissolved in a buffered solution confirm the difference between them (Fig. 4), both in terms of an increased percentage of α-helix content (Table 2) and of a closer similarity with the lysozyme structure in thin film (not shown), compatible with the presence of nanostructured lysozymes in the crystal derived from nanotemplate-based vapor diffusion method, as suggested by recent observations with labeled lysozyme (Pechkova *et al.*, in the press).

The LB crystal turned out superior to the classical crystal with respect to map fragmentation and map correlation to the resulting models. Higher quality of the LB crystal with respect to the classical crystal can again be ascribed to higher water ordering brought about by presence of the film. It should be noted that the technique used for estimating the amount of water in the crystal at this point does not allow taking into account the neighbors of the given lysozyme molecule. With such allowance, the calculated difference is expected to be higher. To achieve this, one needs to combine the simulation technique used herein with the existing tools for unit-cell modelling. Such software adaptation is now in progress.

To summarize, we have shown that even with the small difference in structures of lysozyme molecule itself, LB crystals show pronounced difference in water structure and α-helix content as confirmed by independent circular-dichroism data (Fig. 4), most likely due to the presence in the LB-based crystal of the highly packed and structured lysozymes present in the film (Nicolini, 1977) or alternatively *via* hydrogen-bonding alteration in water caused by either direct hydrogen bonding with the residues of the film exposed to water, or *via* a lattice-like pattern of electric field imposed by the film. We must stress that we have chosen the 'textbook' crystallization protein, lysozyme, to see if the nanocrystallization technique earlier proposed by us could affect crystal quality, in either direction. Considering the already exceptional quality of classical lysozyme crystals, the expected effect could well be negative. Instead, we obtained, even if small, improvement of lysozyme crystal quality, most likely by improving hydrogen-bonding patterns. For proteins that do not crystallize as easily *e.g.* mammalian cytochromes P450, this technique could prove to be an indispensable crystallization tool.

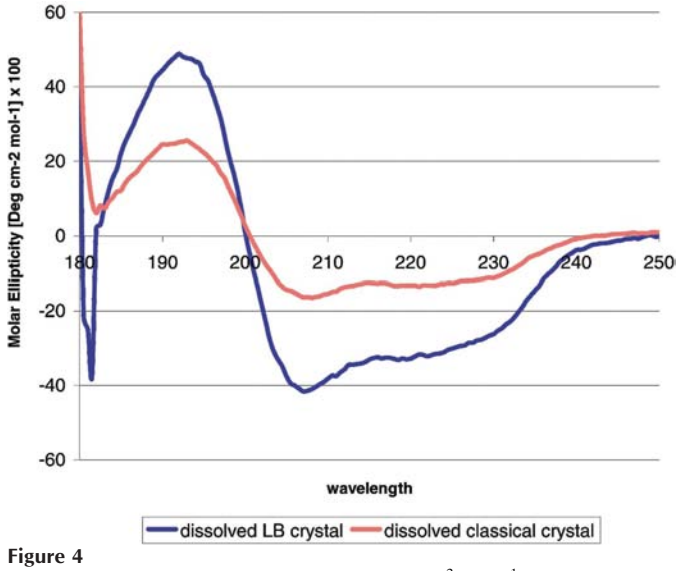

Figure 4
Circular-dichroism spectra in molar ellipticity (deg cm^2 dmol^{-1}) *versus* wavelength (nm) of dissolved lysozyme crystals prepared with (dark blue) and without (light red) nanotemplate-based vapour-diffusion method. A colour version of this figure is available in the online edition of the journal.

This project was supported by a FIRB Grant to the Fondazione Elba and to the Nanoworld Institute of the University of Genova by the MIUR on Organic Nanosciences and Nanotechnologies, by a FISR Grant on Nanotechnology by MIUR to Fondazione Elba and by a Grant on Nanotechnology to the Fondazione Elba by CNR of Italy. The authors are thankful to Professor G. Zanotti (University of Padova, Italy) and to Professor S. Nikonov (Institute for Protein Research, Russian Academy of Sciences) for valuable discussion.

References

Adachi, H., Takano, K., Matsumura, H., Inoue, T., Mori, Y. & Sasaki, T. (2004). *J. Synchrotron Rad.* **11**, 121–124.
Agena, S. M., Pusey, M. L. & Bogle, I. D. (1999). *Biotechnol. Bioeng.* **20**, 144–150.
Arslanov, V. V. (1992). *Adv. Colloid Interface Sci.* **40**, 307–370.
Ataka, M. & Wakayama, N. I. (2002). *Acta Cryst.* D**58**, 1708–1710.
Aurora, R., Creamer, T. P., Srinivasan, R. & Rose, G. D. (1997). *J. Biol. Chem.* **272**, 1413–1416.
Bavastrello, V., Stura, E., Carrara, S., Erokhin, V. & Nicolini, C. (2004). *Sens. Actuators B Chem.* **98**, 247–253.
Bertoncello, P., Nicolini, D., Paternolli, C., Bavastrello, V. & Nicolini, C. (2003). *IEEE Trans. Nanobiosci.* **2**, 124–132.
Bertoncello, P., Notargiacomo, A. & Nicolini, C. (2004). *Polymer*, **45**, 1659–1664.
Bessho, Y., Ataka, M., Asai, M. & Katsura, T. (1994). *Biophys. J.* **66**, 310–313.
Boggon, T. J., Helliwell, J. R., Judge, R. A., Olczak, A., Siddons, D. P., Snell, E. H. & Stojanoff, V. (2000). *Acta Cryst.* D**56**, 868–880.
Brünger, A. T., Adams, P. D., Clore, G. M., DeLano, W. L., Gros, P., Grosse-Kunstleve, R. W., Jiang, J.-S., Kuszewski, J., Nilges, M., Pannu, N. S., Read, R. J., Rice, L. M., Simonson, T. & Warren, G. L. (1998). *Acta Cryst.* D**54**, 905–921/
Chayen, N. E., Saridakis, E., El-Bahar, R. & Nemirovsky, Y. (2001). *J. Mol. Biol.* **312**, 591–595.
Dobrianov, I., Finkelstein, K. D., Lemay, S. G. & Thorne, R. E. (1998). *Acta Cryst.* D**54**, 922–937.
Dobrianov, I., Kriminski, S., Caylor, C. L., Lemay, S. G., Kimmer, C., Kisselev, A., Finkelstein, K. D. & Thorne, R. E. (2001). *Acta Cryst.* D**57**, 61–68.
Felts, A. K., Harano, Y., Gallicchio, E. & Levy, R. M. (2004). *Proteins*, **56**, 310–321.
Forsythe, E. L., Maxwell, D. L. & Pusey, M. (2002). *Acta Cryst.* D**58**, 1601–1605.
Garcia-Ruiz, J. M. (2003). *J. Struct. Biol.* **142**, 22–31.
Grandi, C., Smith, R. E. & Luisi P. L. (1981). *J. Biol. Chem.* **256**, 837–843.
Hu, Z. W., Thomas, B. R. & Chernov, A. A. (2001). *Acta Cryst.* D**57**, 840–846.
Izumi, M., Ohnuki, H., Kato, R., Imakubo, T., Nagata, M., Noda, T. & Kojima, K. (1998). *Thin Solid Films*, 327–329, 14–18.
Judge, R. A., Forsythe, E. L. & Pusey, M. L. (1998). *Biotechnol. Bioeng.* **59**, 776–785.
Judge, R. A., Jacobs, R. S., Frazier, T., Snell, E. H. & Pusey, M. L. (1999). *Biophys. J.* **77**, 1585–1593.
Kadowaki, A., Yoshizaki, I., Rong, L., Komatsu, H., Odawara, O. & Yoda, S. (2004). *J. Synchrotron Rad.* **11**, 38–40.
Kierzek, A. M. & Zielenkiewicz, P. (2001). *Biophys. Chem.* **91**, 1–20.
McRee, D. E. (1992). *J. Mol. Graph.* **10**, 44–46.
Madhusudan, Kodandapani, R. & Vijayan, M. (1993). *Acta Cryst.* D**49**, 234–245.
Manno, M., Xiao, C., Bulone, D., Martorana, V. & San Biagio, P. L. (2003). *Phys. Rev. E*, **68**, 011904.
Nicolini, C. (1998). *Ann. N. Y. Acad. Sci.* **864**, 435 441.
Nicolini, C. (1997). *Trends Biotechnol.* **15**, 395–401.
Nicolini, C. & Baserga, R. (1975). *Biochem. Biophys. Res. Commun.* **64**, 187–195.
Pechkova, E. & Nicolini, C. (2001). *J. Cryst. Growth*, **231**, 599–602.
Pechkova, E. & Nicolini, C. (2003). *Proteomics and Nanocrystallography*, pp. 1–210. Kluwer–Plenum.
Pechkova, E. & Nicolini, C. (2004*a*). *J. Cell. Biochem.* **91**, 1010–1020.
Pechkova, E. & Nicolini, C. (2004*b*). *Trends Biotechnol.* **22**, 117–122.

Pechkova, E., Tropiano, G., Riekel, C. & Nicolini, C. (2004). *Spectrochimica Acta B*, **59**, 1687–1693.
Pechkova, E., Zanotti, G. & Nicolini, C. (2003). *Acta Cryst.* D**59**, 2133–2139.
Penkova, A., Chayen, N., Saridakis, E. & Nanev, C. N. (2002). *Acta Cryst.* D**58**, 1606–1610.
Pepe, I. M. & Nicolini, C. (1996). *J. Photochem. Photobiol. B Biol.* **33**, 191–200.
Pulsinelli, E., Vasile, F., Vergani, L., Parodi, S. & Nicolini, C. (2003). *Protein Pept. Lett.* **10**, 541–549.
Sanjoh, A., Tsukihara, T. & Gorti, S. (2001). *J. Cryst. Growth*, **232**, 618–628.
Tachibana, M., Koizumi, H., Izumi, K., Kajiwara, K. & Kojima, K. (2003). *J. Synchrotron Rad.* **10**, 416–420.
Tsekova, D., Dimitrova, S. & Nanev, C. N. (1999). *J. Cryst. Growth*, **196**, 226–233.
Woerd, M. van der, Ferree, D. & Pusey, M. (2003). *J. Struct. Biol.* **142**, 180–187.
Wild, D. L., Tucker, P. A. & Choe, S. (1995). *J. Mol. Graph.* **13**, 291–298.
Yoshizaki, I., Kadowaki, A., Iimura, Y., Igarashi, N., Yoda, S. & Komatsu, H. (2004). *J. Synchrotron Rad.* **11**, 30–33.